Resolution Analysis Using Fully 3D Electrical Capacitive Tomography

Z. Ye[a], HY Wei[a,b], M. Soleimani[a]

[a] Engineering Tomography Laboratory (ETL) Department of Electronic and Electrical Engineering, University of Bath, Bath, UK. Emails: m.soleimani@bath.ac.uk

[b] Industrial process tomography limited ITS, Manchester, UK

Abstract-Electrical capacitance tomography (ECT) is a non-invasive imaging technique capable of imaging dielectric permittivity contrast of an object. The ECT image reconstruction uses measured capacitance data between pairs of electrode surrounding the object. In some practical ECT applications full access to the surrounding of the object may not be available. In most popular application in ECT for imaging industrial flow through a pipe, there will be missing data from two sides in direction of flow. Another example is a planar array ECT than can have access only to one side of the sample under test. In this paper, a fully 3D array ECT system is developed on six sides of a cubic geometry providing a full access to the imaging region. This fully 3D sensor is used to analyse image quality degradation as a result of missing sides. The sensor development, practical implication, comparison of results with different level of missing data is presented. The resolution analysis is proposed based on theoretical analysis of resolution matrix as well as using singular value decomposition of the Jacobian matrix. The paper presents a number of tools to analyse and quantify the image quality and information that can be achieved in image reconstruction process. The quality of the reconstructed images from experimental data is compared using image resolution parameter for various level of missing data and the results clearly showed how image quality drops with missing information.

Keywords: 3D electrical capacitance tomography, image resolution analysis, volumetric electrical capacitance tomography

1 Introduction

Electrical Capacitance tomography (ECT) is a type of imaging technique, which has been developed for industrial process tomography applications since the late 1980s and early 1990s [1,2,3,4]. ECT is capable of generating permittivity maps inside a nonconductive object by measuring the inter-electrode capacitances for all combinations of electrodes usually surrounding the object. This is achieved by systematically applying a potential to an excited electrode and measuring the inter-electrode capacitance between the excited electrode and every other electrodes, whilst ensuring all other electrodes are kept grounded [1,10,17,18]. From the capacitances measurements, an image is then able to be reconstructed by calculating the distribution of the changes in permittivity inside the imaging

area [5]. Nowadays, most ECT systems, which have been developed, have been designed and built using a traditional arrangement of electrodes, where the electrodes are arranged circumferentially around the target object [3,5,6]. This type of arrangement has a circular or rectangular geometry and requires free access around the complete periphery, where 'full or close to full access tomography' can be achieved [1, 5, 7, 8, 10, 17, 18]. Recently, there are growing interests in 3D electrical capacitance tomography [5-8,10,20]. In 3D ECT full access really means, access to all sides of the object that could allow for volumetric permittivity imaging [17,18,23], so the term fully 3D is used where the electrodes are surrounding all sides of the imaging objects. In that sense, most of the 3D ECT system proposed don't have a full access to the object, such as pipeline multiphase flow imaging or non-destructive evaluation methods. In this paper a fully 3D sensor system is used to analyse the limited access data. For example, in [24] authors have presented a flexible impedance analyser based ECT measurement system and switching system allowing large number of sensors. Such a system could be used in large number of electrodes (96 electrodes) in fully 3D sensor presented in [17]. The same method was adapted in [23] for data collection in fully 3D sensor. In traditional pipeline flow imaging access is missing from two sides. There has also been growing interest in planar array ECT for several new application areas in past few years [11-16, 19]. Limited access tomography is of great importance when there is limited access to the materials under testing, consequently, the number of measurements can be collected from materials under testing is comparatively smaller than full access. This will further results in loss in quality of images that can be reconstructed. This paper aims to investigate the missing data effect on the ECT image reconstruction. In order to reconstruct the whole process from a fully access ECT problem to a very limited ECT problem, a cubical ECT model is developed for 3D ECT imaging while the amount of missing information is control by removing planes of sensor is quantitatively evaluated. The quality of the reconstructed images is assessed qualitatively and also quantified using theoretical models such as resolution matrix and singular value decomposition [9]. The ECT imaging is fundamentally a 3D imaging problem. In this paper, the design of the fully 3D ECT will be presented in the beginning while the effect of missing data test will be explained afterwards. Results and discussion of how missing data influences the imaging reconstruction will be discussed at the end of this paper. Fully 3D ECT sensor model was proposed in [17,18] but only computer-simulated models were developed. This paper verifies fully 3D ECT using experimental data, which in turn helps developing better understanding of missing data in limited access tomography.

2 Sensor and system description

Fully 3D ECT sensor was built consists of six 2x2 planar electrodes planes which were constructed using conductive copper tape as shown in figure 1 below. On each plane, the 4 electrodes were arranged in a 2 x 2 matrix array and attached to a plastic square plate with an area surface of 10cm x 10cm and 4mm in thickness as shown in figure 1(a), the length of electrode array is 3.5 cm x 3.5 cm, between electrodes and surrounding area of the sensor array includes grounded conductors. On the back side of the sensor array a metallic shield used to partly shield the planar array from external interferences. By using this design of six planar ECT sensor planes (as shown in figure 1(b)), each planes of the fully 3D ECT system can be removed and reattached easily so as to carry out the analysis and further study how the image quality varies with different amount of missing data. The measurement of capacitance data were carried out by using the ITS M3C commercial system from Industrial Process Tomography, ITS, (http://www.itoms.com/), ITS M3C commercial ECT system where 24 channel capacitance measurements are possible using a sine-wave excitation with frequency of 1 MHz based system which allows capacitance values down to 0.01pF to be resolved. Excitation method 18 V pick-pick AC based sine wave voltage. Signal to noise ratio (SNR) 56dB. Commom mode rejection ration (CMRR) >-120db for 1 MHz. Type of demodulation use is Phase sensitive demodulation Phase shift compensation 0 –360 degree with 0.09 degree resolution and Speed of acquisition: 15 ms/Frame

(a)

(b)

(c)

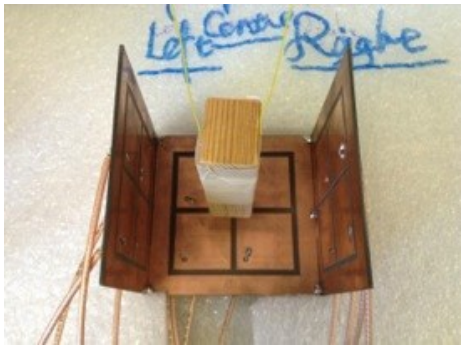

(d)

Figure 1: (a) ECT 3D measurement system (b) Electrode arrangement of one plane of fully 3D ECT system s in the array (c) Inside view of fully 3D ECT system (d) Limited access sensor

3 Computational modelling

To solve the ECT image reconstruction problem the forward simulations are required. In the ECT, the forward problem is the simulation process of calculating the electric potential distribution and capacitances based on the geometric information of the electrical sensor, and excitation and measurement pattern. In a typical ECT real measurement process, the excited electrode is subjected to a sinusoidal voltage while all other electrodes are ground; the total potential is measured on each of the remaining electrodes. All electrodes act as excited electrode in turn similar to the classic circular arrangement. For this reason, the number of measurements has relationship with the number of electrodes given by, $\mathrm{M} = \frac{\mathrm{N}(\mathrm{N}-1)}{2}$, where M is the number of independent measurements and N is the number of electrodes. There are several significant assumptions in the analysis that should be pointed out, namely that it is assumed there are negligible internal charges and wave propagation effects and that the electrostatic approximation $\nabla \times E = 0$, for an electric potential u, and $E = -\nabla u$. According to Poisson's equation the mathematical model for an ECT forward problem can be formulated as,

$$\nabla \cdot (\varepsilon \nabla u) = 0 \ \ on\ \Omega \qquad (1)$$

where ε is the dielectric permittivity, u is the potential, and Ω indicates the region including electrodes, shielding and the imaging region. The electric potential is fixed on each electrode and the boundary conditions can be defined as $u = v_k$ on Ω, where v_k is the voltage signal which is applied on the excited electrode and is zero on all other sensing electrodes. Capacitance of electrode k can be expressed as below,

$$C = \frac{Q_k}{v_k} = \frac{1}{v_k}\int_{\Omega_k} \varepsilon \frac{\partial u}{\partial n} dx^2 \qquad (2)$$

Where n is the inward normal on the electrode number k. The finite element method can be used to satisfactorily solve this problem [6].

Figure 2 shows both sensor model and the meshed model generated by Netgen [21] with the same geometry as the experimental sensor; number of elements in this meshed model is 81834**.** By solving the forward model it is possible to evaluate the capacitance data, which then can be used in inverse problem.

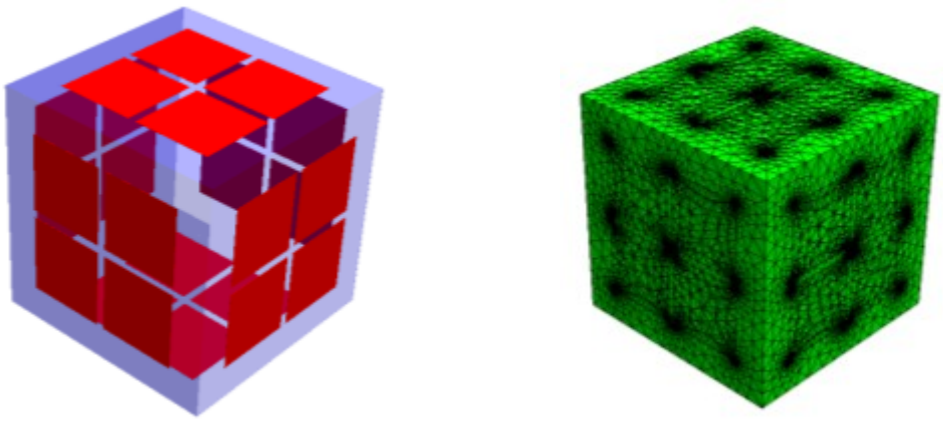

(a) (b)

Figure 2: (a) Computer model of fully 3D ECT Sensor (b) Meshed model for the Fully 3D ECT system

Proposed sensor has 24 electrodes hence there are 276 possible measurements. The relationship between measured data capacitance and the permittivity of each voxel is non-linear; therefore a Jacobian matrix is used to linearize this relationship. Each row of the Jacobian matrix represents the sensitivity of one measurement data with respect to all voxels. Each row of the Jacobian matrix (also called the sensitivity map) indicate the relationship between capacitance and the permittivity of each combinations of electrodes [1,7]. The sensitivity map can be calculated using an efficient formulation based on calculated fields from excitation and sensing electrodes [2].

$$\frac{\partial C_{ij}}{\partial \varepsilon} = -\int_{\Omega} \nabla u_i \nabla u_j dx^3 \qquad (3)$$

where u_i and u_j are potential over region Ω when electrodes i and electrode j are excitation electrodes respectively. Examples of sensitivity plots for some combination of excitation and sensing electrodes are shown in figure 3.

The capacitance measurements between different combinations of pairs of electrodes can be defined as a nonlinear function of the permittivity distribution. Hence **C**=**F**(ε), where **C**=[$C_{1,2}$(ε)... $C_{1,N}$(ε), $C_{2,3}$(ε)…$C_{N-1,N}$(ε)]^T and is the capacitance vector consisting of all capacitance measured of all possible combinations of two electrodes, N is the number of electrodes and **F**(ε)=[f_1(ε)… f_m(ε)… f_M(ε)…]^T. Here, M is the number of measurements. $\boldsymbol{\varepsilon}=[\varepsilon_1, \ldots \quad \ldots$ K is the vector of permittivity distribution which includes K voxels of permittivity. Therefore, the change in capacitance, ΔC, in response to a perturbation of the permittivity distribution, $\Delta\varepsilon$, according to equation 2, the Jacobian matrix can be defined as follows:

$$\Delta C = J \cdot \Delta\varepsilon + O(\Delta(\varepsilon)^2) = \begin{bmatrix} \frac{\partial f_1(\varepsilon)}{\partial \varepsilon_1} & \frac{\partial f_1(\varepsilon)}{\partial \varepsilon_2} & \cdots & \frac{\partial f_1(\varepsilon)}{\partial \varepsilon_k} & \cdots & \frac{\partial f_1(\varepsilon)}{\partial \varepsilon_K} \\ \vdots & \vdots & \ddots & \vdots & \ddots & \vdots \\ \frac{\partial f_m(\varepsilon)}{\partial \varepsilon_1} & \frac{\partial f_m(\varepsilon)}{\partial \varepsilon_2} & \cdots & \frac{\partial f_m(\varepsilon)}{\partial \varepsilon_k} & \cdots & \frac{\partial f_m(\varepsilon)}{\partial \varepsilon_K} \\ \vdots & \vdots & \ddots & \vdots & \ddots & \vdots \\ \frac{\partial f_M(\varepsilon)}{\partial \varepsilon_1} & \frac{\partial f_M(\varepsilon)}{\partial \varepsilon_2} & \cdots & \frac{\partial f_M(\varepsilon)}{\partial \varepsilon_k} & \cdots & \frac{\partial f_M(\varepsilon)}{\partial \varepsilon_K} \end{bmatrix} \cdot \Delta\varepsilon + O(\Delta(\varepsilon)^2) \quad (4)$$

where **J** is the Jacobian matrix of capacitance with respect to permittivity, which is also known as the sensitivity matrix. Elments of the Jacobian matrix are calculated using effiecient sensitivity formula from equation (3). Each row of the Jacobian matrix represents the change of a given measurement as a result of change in permittivity of each voxels. Each column of the Jacobian matrix represents change in all simulated capacitance measurement when a the permittivity of a given voxle has changed. Within the Jacobian matrix in (4), $\frac{\partial f_m(\varepsilon)}{\partial \varepsilon_k}$ indicates the change of the mth capacitance due to the change in permittivity at the k^{th} voxels.

(a) (b) (c)

Figure 3: Sensitivity between electrodes: (a) neighbouring plane (b) between opposite plane (c) between opposite plane in diagonal direction

The inverse problem of this process was achieved by using Tikhonov based method, which is a commonly used algorithm to solve the inverse problem in ECT [2,13]. As stated, the main task of image reconstruction for electrical capacitance tomography is to determine the permittivity distribution from the measured capacitance. In the discrete form, it is necessary to find the unknown $\Delta\varepsilon$ from the known ΔC, while J acts as a constant coefficients matrix in linear image reconstruction cases. In this study an iterative reconstruction method called Tikhonov method was used [13]

$$\Delta\varepsilon = (\mathrm{J}^{\mathrm{T}}\mathrm{J} + \alpha^2\mathrm{R})^{-1}\mathrm{J}^{\mathrm{T}}\Delta\mathrm{C} \qquad (5)$$

Where R is the regulation identity matrix the diagonal elements of Hessian matrix (J^TJ), where J^T is the transpose of the Jacobian matrix, is used as the regularisation term. The regularisation parameter α^2 is chosen empirically 0.1 for full tomography data set, the regularisation parameter was reduced gradually for limited access data. The regularisation parameter for missing side was reduced systematically by rate which the $||\Delta C||_2$ changed (reduced by missing sides).

4 Experimental Results

In this section experimental results will be presented using fully 3D ECT sensor and also when data are missing. The missing data are systematically removed representing missing side. Extensive ranges of experiments were carried out, but here a selection of the results

representing these experiments is shown. In addition to experimental results we have carried out extensive simulation studies. Here resolution analysis for experimental data are shown.

4.1 Fully 3D experiments:

Several experiments were carried out using fully 3D sensor, including single and multiple inclusions. Result shows moving one sample inside the sensor cube. Figure 4 shows image reconstruction for fully 3D experimental data when a cylindrical rubber cork, 2.5cm diameter and 3.0cm height, is moving inside the cubic sensor area from top front corner to the bottom back corner. Figure 5 shows reconstruction of multiple inclusions, two cork were used, and also reconstruction of fully 3D ECT as level detector, where 20% and 60% of cube was filled with Polymer Beads.

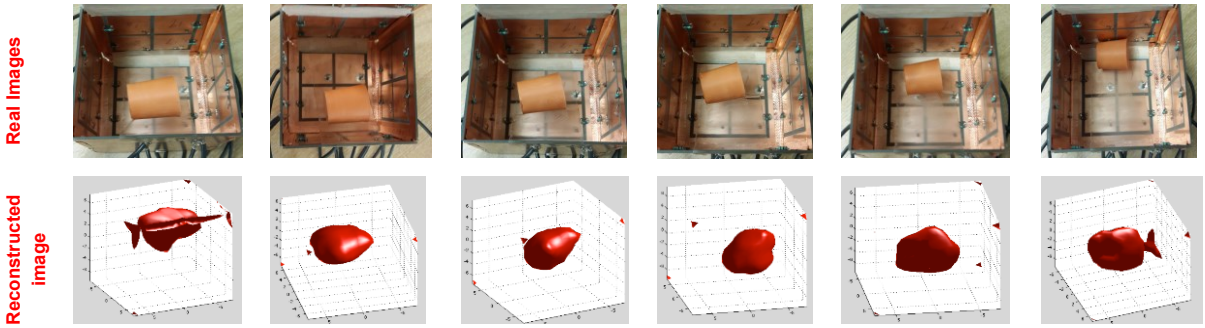

Figure 4: Sample and fully 3D reconstruction of a moving rubber cork

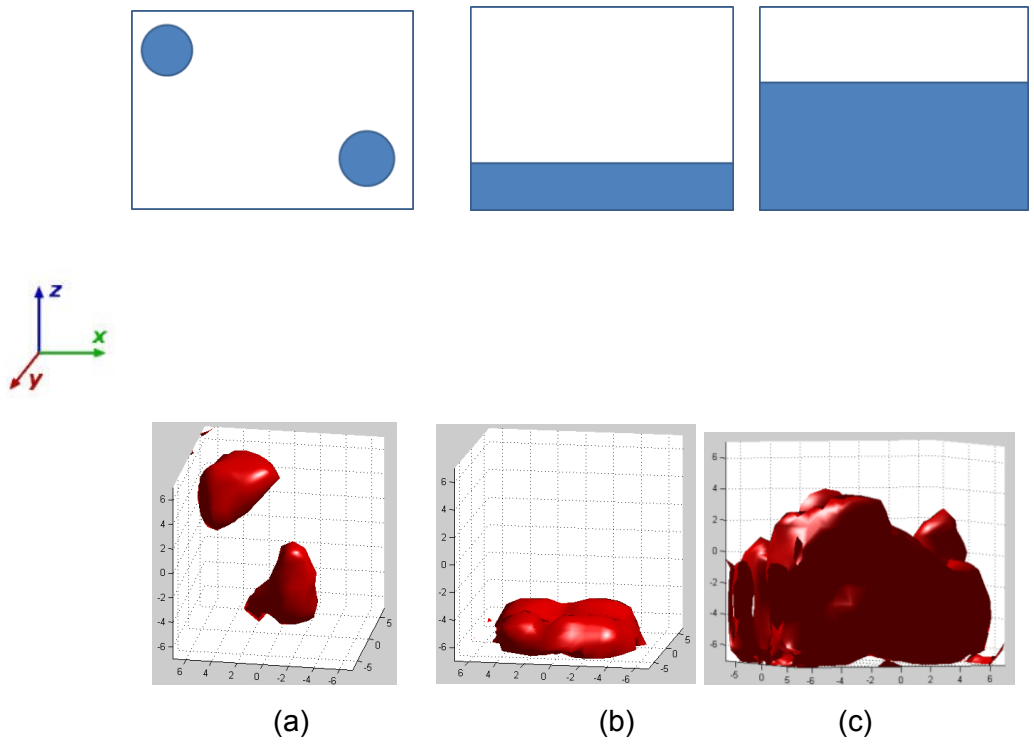

Figure 5: (a) Reconstruction of multiple inclusions in diagonal corners, (b) level detection using fully 3D ECT (20% filled), (c) level detection using fully 3D ECT (60% filled),

4.2 Limited access 3D ECT:

In order to analyse the effect of missing data we have removed data from fully 3D ECT data to make limited access tomography. Figure 6 shows missing sided for limited access tomography. It is worth noticing that the outer shield assumed to remain in all missing data scenario and that may not be possible in realistic limited access ECT cases.

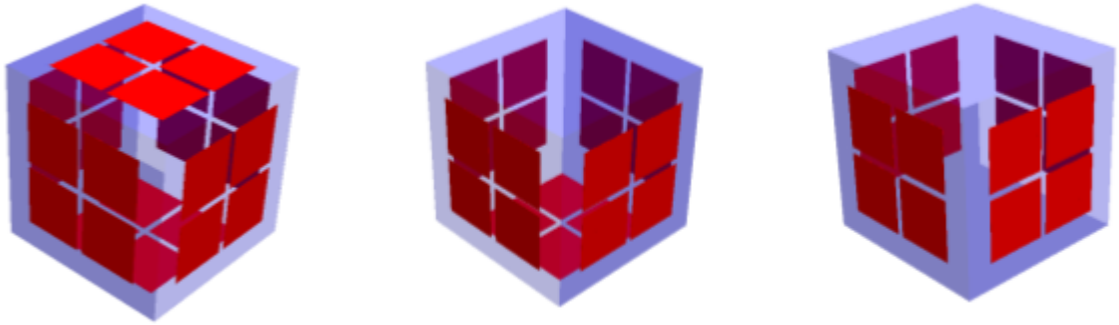

Fully 3D 6 Face Scan | 5 Face Scan | 4 Face Scan

3 Face Scan 2 Face Scan 1 Face Scan

Figure 6: Fully 3D scan and missing sides scan guide

With respect to figure 6, the results of imaging reconstruction are shown in figure 7 for the rubber cork located in centre of imaging region. Here, the experimental results are presented for reconstructed results with missing side from fully 3D ECT system. Figure 6 shows reconstruction of a cork in the central imaging area. The central area is selected, as it is not biased towards any plane. For limited access data, the plates that are not in use are removed. It is important that the degradation of the imaging results when more than three sides are missing should be considered in context of low number of electrodes in this study. The image quality degradations will be further quantified and evaluated in next section. It is worth highlighting the case 6.e when there is missing sides, the remaining 3 face scan is assymetrical making the recovery of corck shape more challenging that one would expect. The same challenge appears in case 6.g which is not only due to lack of symmetry but also sever loss of information due to very limited measured data. If two neighboring planes were selected for 2 face scan image quality will not be as good as 6.f. This is partialy because for assymetrical case there are more sever non-uniformity makes it difficult for traditional regularisation methods to work.

(a)

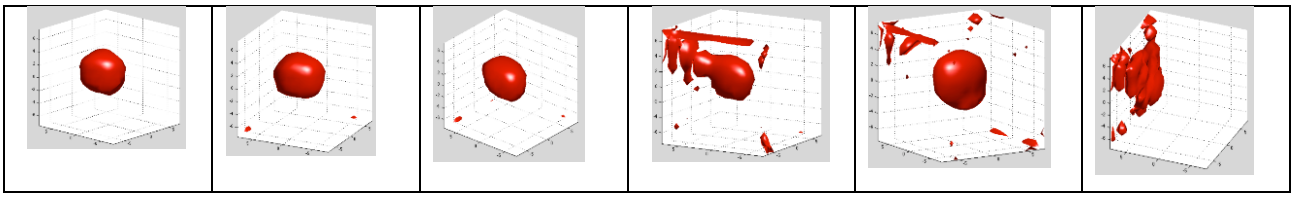

(b) (c) (d) (e) (f) (g)

Figure 7 Image reconstruction results for object in the centre with missing sides. (a) Rubber cork in centre, (b) no missing data with 24 electrodes remaining, (c) one side is missing with 20 electrodes remaining, (d)two sides are missing with 16 electrodes remaining, (e) three sides missing with 12 electrodes remaining, (f) four sides missing with 8 electrodes remaining, and (g) five sides missing, with 4 electrodes remaining

5 Resolution analyses

To be able to verify the effect of missing sides we have adapted three approaches. The first one is relying on singular value decomposition of the Jacobian matrix and by monitoring the trend of singular value decay in difference missing data scenario [9]. The second method is based on analysis of resolution matrix [23], which provides an indication for uniformity of overall sensitivity is different area of interest for imaging. The third method is based on image quality analysis from actual reconstructed images [22].

5.1 Singular Value Decomposition

The singular value decomposition (SVD) is considered as an invaluable tool for analysis of problems with ill-posed matrices and the truncated SVD method has been widely used successfully to solve a variety of discrete ill-posed problems. Hence, in order to determine how image quality varies with different amount of missing data, singular value decomposition is used in this paper as a method of analysis for missing information.

Any matrix $A \in R^{nxm}$

$$A = U\Lambda V^T \qquad (6)$$

Where $U^T U = V^T V = V V^T = I_n$. and $\Lambda \in R^{nxm}$ is a rectangular matrix with the singular values on its main diagonal and zero elsewhere.

A direct approach to the SVD, due to the physicist Lanczos, is to make a symmetric matrix out of the rectangular matrix A as follows:

$$S = \begin{bmatrix} 0 & A \\ A^T & 0 \end{bmatrix} \qquad (7)$$

Since A is in R^{nxm}, S must be in $R^{(n+m)x(n+m)}$

then the eigenvalue problem for S reduces to two coupled eigenvalue problems, one for A and one for A^T

Singular value decomposition of the Jacobian matrix provides an important tool to analyse the behaviour of the underlying inverse problem [9]. Singular value decomposition of the Jacobian matrix in the ECT system shows the potential advantages that the system is able to provide. In these ill-posed problems, ECT requires regularization. The amount of information that can be extracted from the imaging problem depends on the number of singular values that are above the noise level. Based on the Picard criteria, only the singular values above the noise level will contribute to the results.

Figure 8 shows singular value decay for fully 3D and all missing sides. It can be seen that by missing side the slope of the singular value shows more rapid drop showing more severity of the ill-posedness of the inverse problem. For a given noise level in measurement system, the fully 3D have larger number of singular values above the noise comparing to the missing sides.

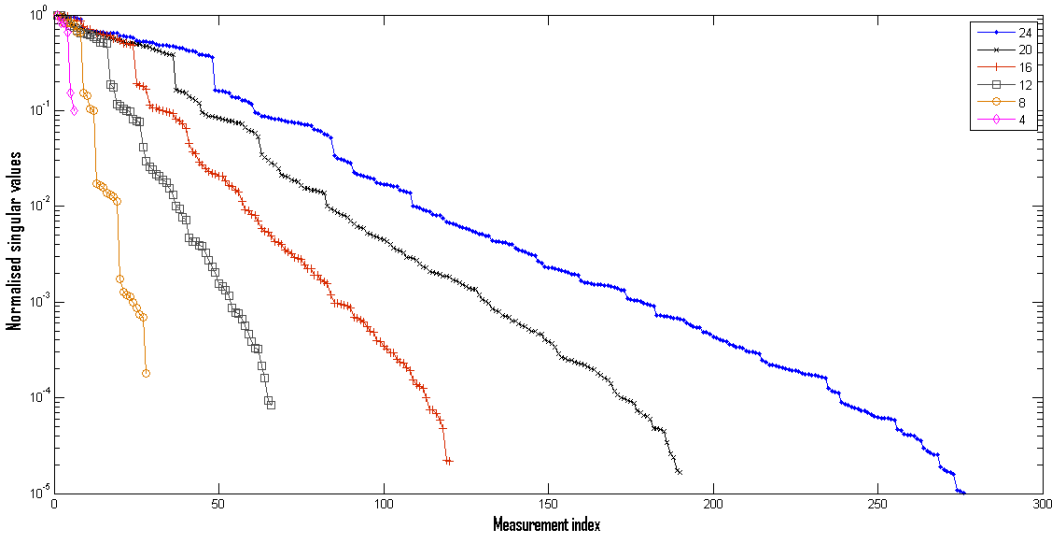

Figure 8: Singular value plot for full data and missing sides

5.2 Resolution Matrix Method:

The reliability of the inverted result could be very limited based on amount of missing information, especially zones where data are totally missing. In order to compare the quality of reconstructed results in a quantity way, the resolution, which identifies where the inversion has a good reliability and where it has not, is using in this paper. Taking the equation $\Delta C = J\Delta\varepsilon_{true}$ and substitute into the inversion equation (5), leading to

$$\Delta\varepsilon = \left(J^T J + \alpha^2 R\right)^{-1} J^T J \Delta\varepsilon_{true} \qquad (7)$$

From (5), the definition of the model resolution matrix R_m can be obtained

$$R_m = (J^T J + \alpha^2 R)^{-1} J^T J \qquad (8)$$

In ideal scenario, the resolution matrix R_m will be identity matrix. Figure 9a, 9b show a plot of diagonal values of matrix R_m for full data and for the case with 3 face scan. The diagonal values are normalised against the largest values. For a matrix of 9261 by 9261 then in an ideal scenario the sum of diagonal values should be 9261. Due to ill-possedness of the inverse problem, in fully 3D ECT the sum of the diagonal values of the matrix R_m is 2000 and will gradually decrease with missing sides as shown in figure 9c. Results in figure 8 shows that various voxels (and regions) are not detectable in the same ways. The variation in detectability is decreasing with the missing side. Figure 9a shows that even with fully 3D data access all area of imaging cannot be reconstructed with the same accuracy, as it is also shown in figure 4. The diagonal elements of the R_m matrix are normalised against their largest value to make it simple to compare the level of homogeneity for reconstructed images for different amount of missing data. Overall level of reconstruction capability can be also evaluate wit the absolute value of the regularisation matrix and will depend on regularisation parameter, but this paper is mostly focusing on comparision for missing data. Additional information such as time correlated imaging in 4D ECT can help to more consistent reconstruction of a moving object [25].

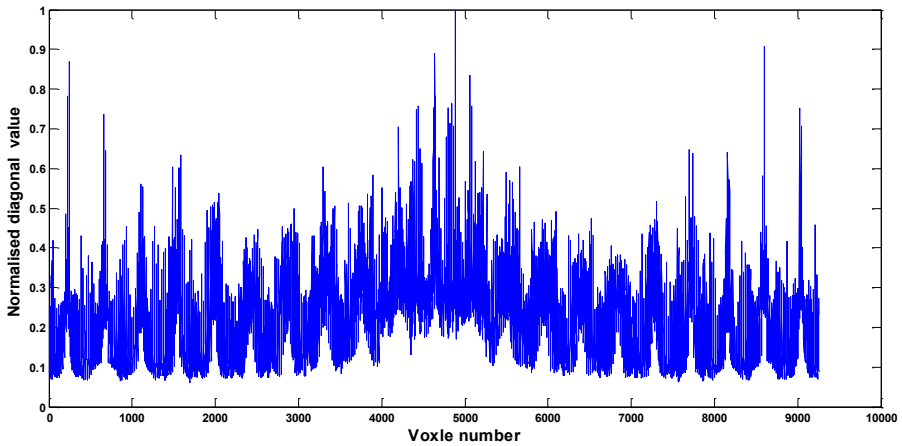

(a)

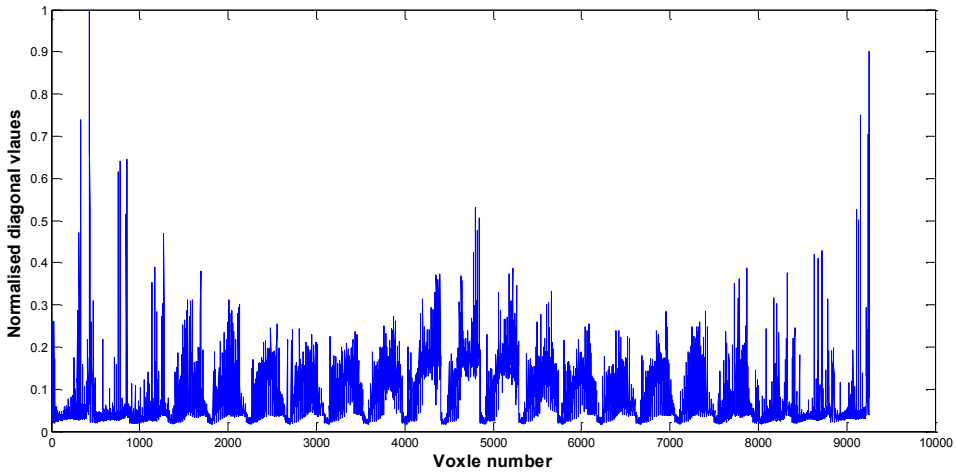

(b)

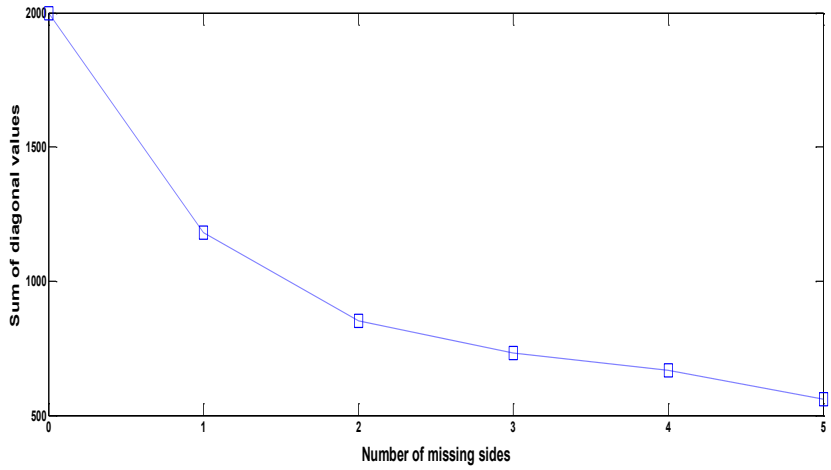

(c)

Figure 9: (a) And (b) Normalised diagonal value of the resolution matrix for full data and 3 face scan, (c) sum of diagonal values against number of missing sides

5.3 Image quality measures

Resolution (RES) measures the size of reconstructed targets as a fraction of the medium. There is wide variety of image quality parameters that could be used for analysis in this section. RES was selected for its simplicity and also to show correspondent with the resolution matrix analysis as well as SVD. In [17] a shape deformation measure has been used for image quality, which could also be used for this study.

Theoretical indication of resolution loss can be verified by analysing the reconstructed images from experimental data from full and missing data sets. Several image quality measures were presented in [22]; such as resolution (RES), positioning error (PE) and

ringing effect (RNG). In this paper, a modified image quality parameter; normalized resolution (NRES) is used to define the variation of the image quality with the depth. Image resolution which is calculated using the equations defined in [22], measures the ratio of voxels number in inclusions (in the case of the experiments in this paper the wooden sample) to the total voxel number [22]. The total voxel numbers represents the volume of region of interest for imaging. It can be defined as

$$RES = \frac{1}{V}\sum_{k}[\hat{x}_k \geq \frac{1}{4}\max_{j}(\hat{x}_j)] \qquad (8)$$

where $\hat{x}_k$ is each voxel in the reconstruction inclusion and V is the volume in the voxels of the total imaging region in true inclusion sample. The RES value then being normalised against the full data set so relative resolution loss can be presented in out of 1 term. Figure 10 shows the image resolution values RES normalised against the resolution value for full access ECT data, which shows image quality degradation by missing sides.

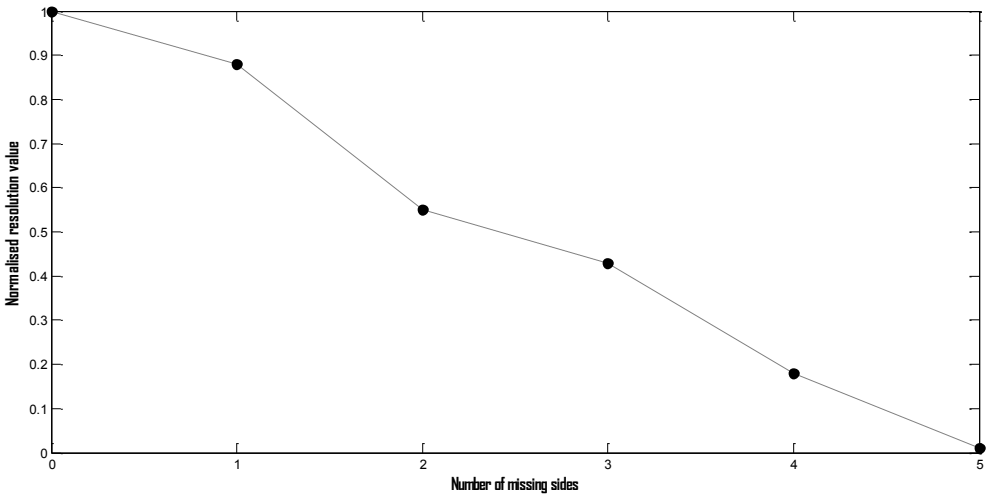

Figure 10: Resolution values for reconstructed images of figure 4

Having been shown in figure 7, when removing more than less than 3 planes, the quality of reconstructed image is still accept, beyond this, the quality became terriblely noisy. When removing less than 3 planes which are shown in figure 6, the fully 3D sensor became a similar transformation of 2 by 8 tridational retangular ECT sensor, which is still able to provide enough information of the location and shape (size) of the test sample by measuring changing in capacitance singal. Beyond this, more sides removing cause in opening non-electrodes region, and accurate information of the test sample is not longer able to be measured via the rest of working electrodes.

With respect to the result, it can be seen the quality of image varies significantly with different level of missing data, furthermore, various analysis methods were used so as to

confirm the conclusion. It can be seen that by increasing missing information the slope of the singular value shows more rapid drop showing more severity of the ill-posedness of the inverse problem. For a given noise level in measurement system, the fully 3D have larger number of singular values above the noise comparing to the missing sides. Furthermore, the resolution values drop sharply with increasing amount of missing information. It is important that the results of this paper is solely focuses on missing sides, and the number of electrodes in each side remain constant and the distance between sides remains constant. Some of these resolution losses may be recoverable by adding electrodes on available sides and also adjusting the distance from the object. The image analysis is carried out for an inclusion in central area of the imaging region to keep the comparisons meaningful for missing sides. Again the image quality may change differently depends on the distance of an inclusion from missing or remaining sides. A wide range of other image quality methods do exsit, which could be used in more specific studies for a different specific requirement for the application.

6 Conclusions

In this paper, a fully 3D sensor was developed and a series of experiments were carried out to analyze how image quality varies with different amount of missing information due to limitted access. Quantitative image quality measures and theoretical tools are used to quantify the effect of missing sides. The paper provides an analyzing tool, which makes it possible to evaluate the effect of missing sides for each imaging scenarios. More evaluations can be carried out in the future studies with larger number of electrodes for example 96 electrodes allowing more realistic scenarios. Future studies could include varying number and shape of electrodes in each side and allowing change of distances between various sides. In many application areas full access to the sample is not possible, but one can quantify how specific 3D imaging geometry may perform for a given application.

Acknowledgement: We thank UK Technology Strategy Board (TSB) to support HY Wei's work on knowledge transfer partnership (KTP) project **(**KTP009034).

References:

[1] Williams, R A, M S Beck, 1995, Process Tomography principles, techniques and applications. Page 52- 53.

[2]Soleimani, M. and Lionheart, W. R. B., 2005, Nonlinear image reconstruction for electrical capacitance tomography using experimental data, Measurement Science and Technology 16. Page 1987-1996.

[3]Yang, W. Q., Peng, L., 2003, Image reconstruction algorithms for Electrical Capacitance Tomography, Measurement Science and Technology, 14. Page R1–R13.

[4]Alme, K. J., Mylvaganam, S., 2006, Electrical Capacitance Tomography—Sensor Models,Design, Simulations, and Experimental Verification, IEEE Sensors 6(5). Page 1256 - 1266

[5]Wajman, R., Banasiak, R., Mazurkiewicz, Ł., Dyakowski, T., Sankowski, D., 2006, Spatial imaging with 3D capacitance measurements, Measurement Science and Technology, vol. 17, no. 8, August 2006, pp. 2113-2118;

[6]Soleimani, M. 2006, Three-dimensional electrical capacitance tomography imaging, Insight, Non-Destructive Testing and Condition Monitoring, Vol. 48, No. 10, Pages: 613-617.

[7]Banasiak, R., Wajman R., Sankowski, D., Soleimani, M., 2010, Three-dimensional nonlinear inversion of electrical capacitance tomography data using a complete sensor model, Progress in Electromagnetics Research 100: 219-234.

[8]Banasiak, R., Wajman R., Sankowski D., Soleimani, M., 2010, Three-dimensional nonlinear inversion of electrical capacitance tomography data using a complete sensor model, PIER 100: 219-234.

[9] Hanson, P. C. 1998. Rank-deficient and discrete ill-posed problems: numerical aspects of liniear inversion, Philadephia, Society for Industrial and Applied Mathematics.

[10]Warsito, W., Development of 3D Electrical Capacitance Tomography based on neural Network Multi-Criterion Optimization Image Reconstruction., 3rd World Congress on Industrial Process Tomography, Banff.

[11] Wang F., Marashdeh Q., Fan, L. and Warsito, W., 2010, Electrical Capacitance Volume Tomography: Design and Applications, Sensors, 10, 1890-1917

[12]Hu, X. H. and Yang, W. Q., 2010, Planar capacitive sensor: designs and applications. Sensor Review. 30(1): 24-39.

[13]Chen, D. X., Hu, X. H. and Yang, W. Q., 2011, Design of a security screening system with a planar single-electrode capacitance sensor matrix, Meas. Sci. and Technol.; 22(11): 114026.

[14]Diamond, G. G., Hutchins, D. A., Gan, T. H., Purnell, P. and Leong, K. K., 2006, Single-sided capacitive imaging for NDT, Insight 48, 724-730.

[15]Yin, X., Hutchins, D. A., 2012, Non-destructive evaluation of composite materials using a capacitive imaging technique, Composites Part B: Engineering, Volume 43, Issue 3, Pages 1282–1292.

[16] Gebrial, W., Prance, R. J., Harland, C. J ., Clark T.D.,2006, Non-Invasive Imaging Using an Array of Electric Potential Sensors. Review of Scientific Instruments, 77. 063708-1 . ISSN 0034-6748.

[17] Soleimani, M., Wang, H., Li, Y. and Yang, W., 2007. A comparative study of three dimensional electrical capacitance tomography. International Journal for Information & Systems Sciences, 3 (2), pp. 292-306.
[18] Ren S., Xu Y., Tan C., and Dong F.,2013, Reconstructing the geometric configuration of three dimensional interface using electrical capacitance tomography, Int. J. Numer. Meth. Engng 2013; 96:628–644
[19]Ye, Z., Banasiak R, and Soleimani M, 2013, Planar array 3D electrical capacitance tomography, Insight, Vol. 55, no.12., pp. 675-680.
[20]Li, Y, and, Holland D, 2013, Fast and robust 3D electrical capacitance tomography, Meas. Sci. Technol. 24 105406.
[21] Schoberl J, 1997, NETGEN An advancing front 2D/3D-mesh generator based on abstract rules, Comput Visual Sci 1:41–52.
[22] Adler A, et al. 2009, GREIT: a unified approach to 2D linear EIT reconstruction of lung images, Physiol Meas, Vol 30, No.6.
[23] Tarantola, A, Inverse Problem Theory and Methods for Model Parameter Estimation, 2nd edition, SIAM.
[23] Ren S, Dong F, Xu Y, and Tan C, 2014, Reconstruction of the three dimensional inclusion shapes using electrical capacitance tomography, Meas. Sci. Technol. 25 025403.
[24] Hu X H, Yang M, Ismail I, Li Y, Yang W Q and Manrique de Lara M, 2008 An impedance-analyser-based multi-channel imaging system and its applications Proc. IEEE Int. Workshop on Imaging Systems and Techniques (Chania, Greece) p 181-6.